Cooperative Catalysis in the Homodimer Subunits of Xanthine Oxidase†

Lin Ai Tai and Kuo Chu Hwang*

Department of Chemistry, National Tsing Hua University, Hsinchu, Taiwan

Received August 15, 2003; Revised Manuscript Received February 14, 2004

ABSTRACT: Xanthine oxidase (XOD) consists of two identical subunits. For the past 50 years or so, it was assumed that the two subunits carry out catalysis *independently*. Herein, we report that the presence of 6-formylpterin (6FP) or other substrates (such as xanthine or xanthopterin) at one of the two active sites affects the binding affinity and catalysis rate of 6FP at the other. When the two XOD active sites were occupied by two 6FPs simultaneously, the conversion rate (2.8×10^{-3} s^{-1}) of 6FP to 6CP is 2.95-fold faster than the conversion rate (0.95×10^{-3} s^{-1}) in the case of single 6FP bound condition. The presence of xanthine can accelerate the catalysis rate of 6FP by XOD as well as the activity-recovering rate of alloxanthine-inhibited XOD. Our experimental observations demonstrate unambiguously that the two XOD subunits are strongly cooperative in both binding and catalysis. The inhibition constant (K_i) of 6FP toward XOD was measured by a stopped-flow method to be 0.94 nM.

Xanthine oxidase (XOD)[1] is a 290 kDa homodimer protein (*1*). In each subunit, there are four cofactors, namely, Mo^{6+}-cofactor, two [2Fe−2S] clusters, and a FAD unit. The Mo^{6+} site can transfer and insert an oxygen atom into the C−H bond of many substrates with concomitant reductive conversion of Mo^{6+} to Mo^{4+}. The reduced Mo^{4+} cofactor then passes two electrons via the two [2Fe−2S] cofactors to the FAD site, converting it to $FADH_2$, which then reduces molecular oxygen to $O_2^{-\bullet}$ or H_2O_2. In addition to xanthine, many biomolecules, such as hypoxanthine, are also substrates of XOD. XOD consists of two identical subunits. During the past 50 years or so, it was always assumed that the two XOD subunits carry out catalysis *independently* (*1*−*3*), despite the observation of substrate inhibition phenomenon at high substrate concentration conditions (*4*, *5*). In the literature, this was observed in many oligomeric enzymes in which cooperativity exists among catalytic subunits (*6*−*9*). Very strong negative cooperativity leads to complete loss of activity in the neighbor subunits, which is known as "half-of-the-sites" reactivity phenomenon (*8*, *9*). Some oligomeric enzymes having lack of cooperativity among subunits were transformed into cooperative forms after a single mutation of an amino acid near active sites (*10*−*12*). For example, it was reported that deletion of the C-terminal extension of phosphofructokinase converts the enzyme from nonallosteric to allosteric (*13*). Replacement of an amino acid (Cys-509) by tyrosine or serine converts *Penicillium chrysogenum* ATP sulfurylase from an allosteric enzyme that requires the presence of an allosteric effector, 3′-phosphoadenosine 5′-phosphosulfate (PAPS) to an intrinsically cooperative one at pH 8 in the absence of the allosteric effector (*14*). Chemical treatment of *Clostridium symbiosum* glutamate dehydrogenase by β-mercaptoethanol leads to activation of five subunits that otherwise are inactive and also results in positive cooperative interactions among the six catalytic subunits of the enzyme (*15*). Replacement of an amino acid, Arg-475, by glutamine converts the cooperativity of aldehyde dehydrogenase from extreme negative cooperativity (i.e., half-of-the-sites reactivity) to positive cooperativity (*16*). In the case of human glutathione transferase P1-1 (EC2.5.1.18), replacement of Cys-47 with alanine or serine decreases the affinity for GSH and triggers a positive kinetic cooperativity with respect to the substrate (*17*). Another example is NAD^+-dependent isocitrate dehydrogenase from *Saccharomyces cerevisiae*, which is an octamer composed of two hetero-subunits, IDH1 and IDH2 (*18*). Replacement of a serine residue by alanine at the active site of IDH1 results in a 6-fold decrease in the V_{max} and a decrease in cooperativity but little change in the $S_{0.5}$ for isocitrate. If the same replacement occurs in the IDH2 subunit, a 60-fold decrease in the maximal velocity and a 2-fold reduction in $S_{0.5}$ for isocitrate were observed, but the cooperativity was unaffected. It was also reported that binding of Zn^{2+} ion to *Escherichia coli* ornithine transcarbamoylase (*19*) and mannitol-1-phosphate dehydrogenase (from *Aspergillus parasiticus*) (*20*) converts the oligomeric enzymes from noncooperative to positively cooperative. With so many oligomeric enzymes having cooperativity in mind, it is therefore reasonable to wonder whether cooperativity exists between the two XOD subunits.

In this paper, we provide solid experimental evidence to show that both the binding and catalytic functions of the two XOD subunits are, in fact, highly associated with one another. The presence of a 6-formylpterin (6FP) molecule at one XOD active site accelerates the catalysis rate of 6FP at the other active site. The presence of xanthine can also accelerate the catalysis rate of 6FP by XOD as well as the activity-recovering rate of alloxanthine-inhibited XOD.

† This work was supported by the National Science Council, Taiwan, R. O. C. (Grant NSC 91-2113-M-007-064).

* Corresponding author. Tel/Fax: (886) 3572 4810. E-mail: kchwang@mx.nthu.edu.tw.

[1] Abbreviations: XOD, xanthine oxidase; 6FP, 6-formylpterin; 6CP, 6-carboxylpterin; AFR, activity−flavin ratio; ES, enzyme−substrate complex.

10.1021/bi035467b CCC: $27.50
Published on Web 03/27/2004

MATERIALS AND METHODS

Purification of Enzymes. 6-Formylpterin (6FP, >99%, Lancaster) was used as received. XOD was purchased from Sigma. It is believed that XOD from commercial samples might contain three different forms, namely, a doubly active dimer, a mixed dimer, and a doubly inactive dimer. The inactive unit might be in the desulfo form (*21*) or lack the molybdenum metal (*22*, *23*). By following a literature procedure, XOD was purified using a Sepharose 4B−folate affinity column (*24*). The Sepharose 4B−folate gel was prepared by coupling folic acid with EAH-Sepharose 4B (Pharmacia Biotech) in the presence of EDC [*N*-ethyl-*N*′-(3-dimethylaminopyropl)carbodiimide hydrochloride]. The commercial XOD sample was first dissolved in a 0.1 M phosphate buffer (pH 7.5) and then placed in a centricon centrifugal tube with a 100 K membrane (Millipore, YM-100) to concentrate the enzyme solution under a centrifuging field of 1000 rpm. The solution was then passed through a Sephadex G-25 column to remove small molecules and additives from the enzyme. An excess amount of allopurinol was added to the enzyme solution to convert XOD completely to the form of the alloxanthine−XOD(Mo^{4+}) complex. The alloxanthine−XOD(Mo^{4+}) complex was isolated by passing the solution through a Sephadex G-25 column. The solution was concentrated again to a volume of 0.5 mL before passing through a Sepharose 4B−folate affinity column (0.7 cm × 8 cm). The completely active XOD in the form of the alloxanthine−XOD complex passes through the affinity column more rapidly than the partially active and the completely inactive XODs. The eluted solution was collected in test tubes in volumes of 1 mL each. The absorbance ($A_{450\ nm}$) of each collected sample was measured. The initial seven collected samples contained highly concentrated, fully active XOD and were combined into a test tube. Ferricyanide (1 mM) was added to the concentrated alloxanthine−XOD solution to directly oxidize the Mo^{4+} unit and to dissociate the alloxanthine−XOD(Mo^{4+}) complex (*25*). The solution was passed again through a Sephadex G-25 column. The final solution was concentrated under a centrifuging field to obtain free and active XOD.

The total XOD concentration, $[XOD]_T$, including both active and inactive forms was determined by the UV−visible absorbance at 450 nm with an absorption coefficient, $\epsilon_{450\ nm}$, of 37 800 $M^{-1}\ cm^{-1}$ (*25*). The percentage of functionally active XOD in the purified sample was determined by two methods. The first one is the activity−flavin ratio (AFR) method (*26*, *27*). The AFR value is a ratio of the absorbance at 295 nm of uric acid, which is formed by catalysis of excess xanthine within 1 min, versus the absorbance of oxidized XOD at 450 nm ($A_{450\ nm}$). In the experiments, the absorbance $A_{450\ nm}$ of a purified XOD solution (0.1 M phosphate buffer, pH 8.5, 25 °C) was determined to be 0.200. The stock solution was then diluted 200 times ($A_{450\ nm} = 0.001$), and an aliquot of the enzyme solution was added to an 80 μM xanthine solution at 25 °C. After 1 min catalysis, the measured $A_{295\ nm}$ of uric acid is 0.178. Therefore, the $AFR^{25°C}$ value for the purified XOD sample was 178. According to the literature, the value of the $AFR^{25°C}$ for completely active XOD is 210 (*26*, *27*). Therefore, the sample contains 84.8% (i.e., 178/210) of functionally active XOD enzymes. In addition to the AFR method, the fraction of functionally active XOD can be determined also by the "fast phase" component method (*27*, *28*). In the presence of xanthine and under an anaerobic conditions, the consecutive oxidative catalysis of xanthine by XOD accumulates electrons in the enzyme cofactors and leads to bleaching of the absorbance of XOD at 450 nm. This bleaching (i.e., the reduction of XOD cofactors) displays a distinct two-component (both fast and slow phases) decay pattern (*28*). The percentage of the fast phase was reported to be linearly proportional to the specific activity, or the value of the AFR, of XOD (*27*). In our hands, a solution of the initially eluted XOD sample in 0.1 M phosphate buffer solution (pH 8.5) was preincubated with glucose oxidase (0.13 mg/mL), catalase (0.066 mg/mL), and D-glucose (100 mM) (*29*) for 20 min to remove O_2 from the solution, and then, excess xanthine (200 μM final concentration) was added to reduce the cofactors of XOD. An AFR value of 179 was obtained by comparing the value of $\Delta\epsilon_{450\ nm}$ to the standard curve—a plot of $\Delta\epsilon_{450\ nm}$ as a function of the value of the $AFR^{25°C}$—displayed in Figure 8 of ref *27*. The $AFR^{25°C}$ value of 179 corresponds to a purity of 85%. Thus, based on the two methods, the fraction of active XOD in the purified sample was ca. 85%. The concentration of functional XOD active sites in monomeric form, $[XOD]_{mo}$, was equal to 85% of the total XOD concentration, $[XOD]_T$. The concentration of dimeric XOD, $[XOD]_{di}$, is equal to half of the $[XOD]_{mo}$.

Enzyme Activity Measurements. The XOD activity was measured by addition of an aliquot of the XOD (or alloxanthine−XOD complex) solution to a 100 μM xanthine solution (in 0.1 M phosphate buffer, pH 7.5), followed by measuring the uric acid absorption at 295 nm as a function of time. The $A_{295\ nm}$ was divided by $\Delta\epsilon_{295\ nm}$ between uric acid and xanthine ($\Delta\epsilon_{295\ nm} = 1.13 \times 10^4\ M^{-1}\ cm^{-1}$) and converted to the uric acid concentration. The rate of catalysis of a XOD−6FP solution was divided by the free XOD concentration to express as a normalized activity.

In the stopped-flow experiment (Applied Photophysics, model pistar-180), 40 μM (the concentration of functional active sites) XOD aqueous solution (in 0.1 M phosphate buffer, pH 7.5) was injected into a 6FP (4 μM, 0.1 equiv relative to the XOD functional active site) aqueous solution at 22 °C, and the absorbance at 620 nm was monitored at a sample cell of 0.2 × 0.2 × 1 cm^3 volume with the path length of 1 cm. To avoid the simultaneous binding of two 6FPs to a XOD molecule, all experiments, unless otherwise mentioned, were carried out by adding aliquots of XOD solution into a dilute 6FP solution, instead of the other way around.

RESULTS AND DISCUSSION

Determination of the Value of K_i for the Inhibition of XOD by 6FP. The compound 6FP is a very poor substrate for XOD and can be slowly converted to 6-carboxylpterin (6CP) via enzyme reaction. Mixing 6FP and XOD results in the formation of a 6FP/XOD complex, which has a distinct broadband absorption at 620 nm (*30*). The 620 nm absorbing species was previously assigned to a 6FP−Mo complex, and the amount of the 620 nm absorbance change was directly proportional to the specific activity of the enzyme (*30*). Because of its very slow rate of conversion, 6FP is considered to be a very good inhibitor of XOD. Values of K_i of 6FP for the inhibition of XOD have been reported in the literature

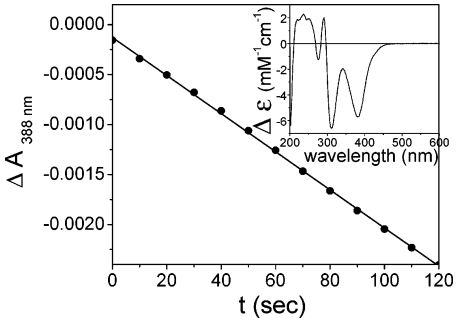

FIGURE 1: The bleaching of a solution of the XOD−$6FP_1$ complex monitored as a function of time in the UV−vis spectra at 388 nm. The XOD−$6FP_1$ complex was prepared by mixing a solution of 40 μM XOD (the concentration of functional active sites) in 0.1 M phosphate buffer (pH = 7.5, 22 °C) with 4.0 μM 6FP. The solid line represents the linear fitting of the decay in the 388 nm absorbance, and the slope is equal to dA/dt. The catalytic rate of 6FP was obtained by dividing the slope by $\Delta\epsilon_{388\ nm}$. The inset displays the (6CP − 6FP) difference spectrum of subtracting the spectrum of 6CP from that of 6FP.

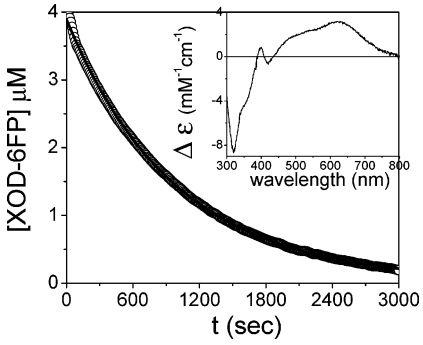

FIGURE 2: The UV−visible decay of a solution of the XOD−$6FP_1$ complex at 620 nm monitored as a function of time. A solution of 40 μM XOD (concentration of functional active sites) in 0.1 M phosphate buffer (pH 7.5, 22 °C) was mixed with 4 μM 6FP (final concentration). The decay of the 620 nm absorbance was monitored 10 s after mixing XOD into the dilute 6FP solution. The decay was fitted to a single-exponential function, $\exp[-(k_2 + k_3)t]$. A ($k_2 + k_3$) value of 1.02×10^{-3} s^{-1} was obtained. The inset displays the difference spectrum by subtracting the spectrum of the XOD−$6FP_1$ complex from the sum of the spectra of individual components, 6FP and XOD.

to be 0.6 (*31*) and 1.78 nM (*32*). These values being obtained by the traditional Lineweaver−Burk plot (1/V vs 1/[S]) are based on the Michaelis−Menten model, which is a kinetic model derived for single site enzymes. The basic assumption in the kinetics of the Michaelis−Menten model is the steady-state approximation condition for the formation and consumption of the enzyme−substrate ([ES]) complex, as well as a rapid equilibration between the reactants (enzyme plus substrate) and the enzyme−substrate complex. Since the dissociation rate of the XOD−$6FP_1$ complex is far too slow (on the order of 10^{-4} s^{-1} at 22 °C, vide infra), the reactants (substrates plus enzymes) are not in dynamic equilibrium with the enzyme−substrate complex on the time scale of ~238 min (vide infra) at 22 °C. Therefore, the Lineweaver−Burk method is not a correct one for measuring accurate values of K_m or K_i for very slowly dissociating substrates, such as 6FP. In this case, it was necessary to deduce a valid process to measure correctly the values of k_1, k_2, and k_3 for inhibition of XOD by 6FP. Based on eq 1, the rate of

$$6FP + XOD \underset{k_2}{\overset{k_1}{\rightleftharpoons}} XOD{-}6FP_1 \xrightarrow{k_3} 6CP + XOD \quad (1)$$

formation (V) of 6CP is equal to k_3 multiplied by the concentration of the enzyme−substrate complex, that is, V = d[6CP]/dt = k_3[XOD−$6FP_1$]. Conversion of 6FP to 6CP will lead to bleaching at 388 nm ($\Delta\epsilon_{388\ nm} = \epsilon_{6CP} - \epsilon_{6FP} = -5380$ M^{-1} cm^{-1}). By mixing 40.0 μM XOD (the concentration of functional active sites, $[XOD]_{mo}$) with 4.0 μM (i.e., 0.1 equiv) 6FP and monitoring the bleaching at 388 nm (i.e., the formation of 6CP) as a function of time, one can obtain the rate of catalysis V = d[6CP]/dt = k_3[ES] = 3.55×10^{-9} M s^{-1} (see Figure 1). Since the conversion of 6FP to 6CP is very slow and the equilibrium constant (k_1/k_2) is very large (ca. 10^{10} M^{-1}, vide infra), binding of 6FP to the XOD active sites is nearly quantitative and irreversible, and the concentration of the enzyme−substrate complex is virtually equal to the concentration of 6FP (i.e., [XOD−$6FP_1$] = 4.0 μM) at the very early mixing time of 6FP and XOD. After 70 s of mixing (i.e., the midpoint of the experiments in Figure 1), the concentration of the [ES] complex is estimated to be 3.73 μM by using the equation $[ES] = [ES]_0\ e^{-(k_2+k_3)t}$ (see eq 4), where a ($k_2 + k_3$) value of 1.02×10^{-3} s^{-1} (see results in Figure 2) is adapted in the calculation. Therefore, $V = k_3[ES] = 3.55 \times 10^{-9}$ M s^{-1}. By treating the [XOD−$6FP_1$] ≒ 3.73 μM, one obtains a k_3 value of 0.95×10^{-3} s^{-1}. The next challenge is to measure the values of k_1 and k_2. From eq 1, the rate of formation of the [ES] complex, d[XOD−$6FP_1$]/dt, is equal to $-(k_2 + k_3)$[XOD−$6FP_1$] + k_1[XOD]-[6FP] or

$$d[XOD{-}6FP_1]/dt = -(k_2 + k_3)[XOD{-}6FP_1] + k_1[XOD][6FP] \quad (2)$$

To obtain the value of ($k_2 + k_3$), 40 μM XOD was mixed with 4 μM (i.e., 0.1 equiv) 6FP to generate the XOD−$6FP_1$ complex. Since binding of 6FP to the XOD active sites is essentially quantitative and irreversible (vide infra), nearly all free 6FP is converted to the XOD−$6FP_1$ complex within a few seconds after mixing XOD with 6FP, and the concentration of free 6FP is negligibly small. Therefore, in the absence of free 6FP, d[XOD−$6FP_1$]/dt becomes equal to the rate of dissociation of the isolated XOD−$6FP_1$ complex, that is,

$$-d[XOD{-}6FP_1]/dt = (k_2 + k_3)[XOD{-}6FP_1] \quad (3)$$

Via rearrangement and integration of eq 3, one obtains

$$[XOD{-}6FP_1] = [XOD{-}6FP_1]_0\ e^{-(k_2+k_3)t} \quad (4)$$

A value for ($k_2 + k_3$) of 1.02×10^{-3} s^{-1} was obtained by fitting the decay of the $A_{620\ nm}$ absorbance of the XOD−$6FP_1$ complex to eq 4 (see Figure 2). Since the value of k_3 is 0.95×10^{-3} s^{-1}, the value of k_2 is thus 0.7×10^{-4} s^{-1} at 22 °C. The value of k_2 is so small that once a XOD−$6FP_1$ complex is formed, it does not dissociate appreciably back to free 6FP and XOD within a time scale of 238 min at 22 °C. The major exit channel of the bound 6FP is enzymatic conversion to 6CP.

To obtain the value of k_1 for the formation of the XOD−$6FP_1$ complex, a stopped-flow mixing experiment was

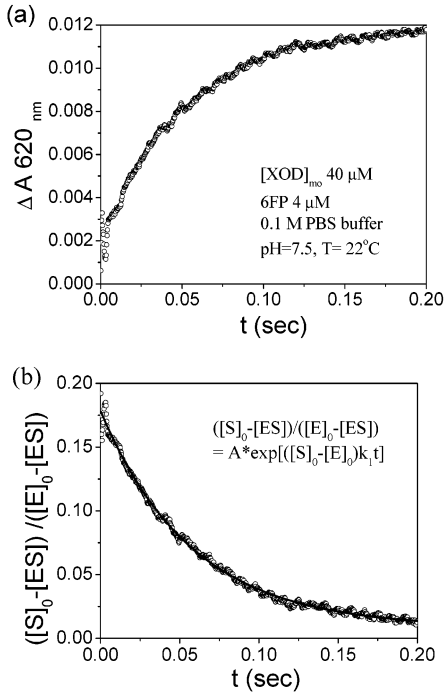

FIGURE 3: The absorbance $\Delta A_{620\ nm}$ (a) plotted as a function of time after mixing 4 μM 6FP with a solution of 20 μM XOD dimer ($[XOD]_{di}$) in 0.1 M phosphate buffer (pH 7.5, 22 °C) in a stopped-flow spectrometer (b) processed to be in the form of $([S]_0 - [ES])/([E]_0 - [ES])$ as a function of the mixing time, t, where $[E]_0$ and $[S]_0$ are the initial concentrations of XOD dimer and 6FP, respectively, and [ES] is the concentration of the XOD−$6FP_1$ complex at time t. The solid line is a fitting curve based on the equation $([S]_0 - [ES])([E]_0 - [ES]) = A \exp[([S]_0 - [E]_0)k_1t]$. The complex formation rate k_1 is obtained to be 1.09×10^6 M^{-1} s^{-1}.

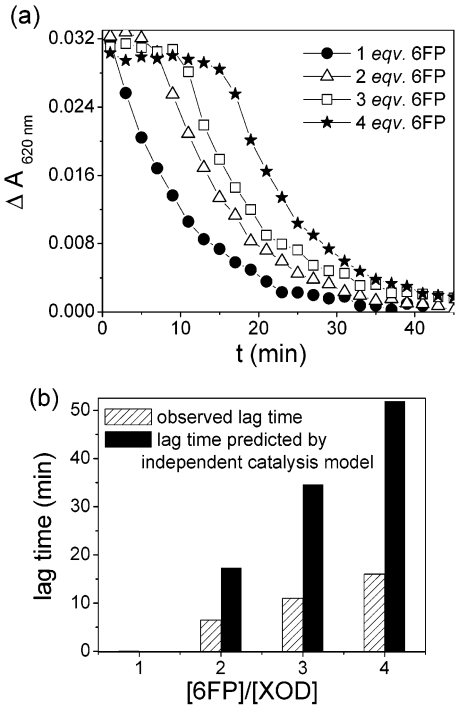

FIGURE 4: Bleaching in the intensity of the 620 nm absorbance (i.e., a measure of the amount of the XOD/6FP complexes) as a function of time (a) in the presence of 1(●), 2 (△), 3 (□), and 4 (★) equiv of 6FP and (b) the observed lag time in panel a and the predicted lag time by the independent catalysis model as a function of the number of equivalents of 6FP. The solution contains 10 μM XOD (concentration of the functional active sites) and different amounts of 6FP in 0.1 M phosphate buffer at pH 7.5 and 22 °C.

undertaken. The rate of complex formation, k_1, can be obtained by mixing XOD with a dilute (e.g., 0.1 equiv) 6FP solution and monitoring in real time the formation of the XOD−$6FP_1$ complex at 620 nm. Based on eq 5 and under

$$E + S \xrightarrow{k} [ES] \qquad (5)$$

the condition of highly dilute 6FP (e.g., 0.1 equiv), each XOD subunit can only bind with a 6FP. One considers the kinetics in Scheme 1. The rate of complex formation, k, can be obtained by fitting the experimental data $([S]_0 - [ES])/([E]_0 - [ES])$ vs time t (see eq 6, Scheme 1), where $[E]_0$ and $[S]_0$

Scheme 1

$$d[ES]/dt = k\,[E][S] = k\,([E]_0 - [ES])([S]_0 - [ES])$$
$$[1/(([E]_0 - [ES])([S]_0 - [ES]))]\,d[ES] = k\,dt$$
$$\int[1/(([E]_0 - [ES])([S]_0 - [ES]))]\,d[ES] = \int k\,dt$$
$$\int[1/([S]_0 - [E]_0)][1/([E]_0 - [ES]) - 1/([S]_0 - [ES])]\,d[ES] = \int k\,dt$$
$$[1/([S]_0 - [E]_0)]\ln([S]_0 - [ES])/([E]_0 - [ES]) = k\,t$$
$$\ln([S]_0 - [ES])/([E]_0 - [ES]) = ([S]_0 - [E]_0)\,k\,t + A$$
$$([S]_0 - [ES])/([E]_0 - [ES]) = A*\exp([S]_0 - [E]_0)\,k\,t \qquad (6)$$

are the initial concentrations of the XOD functional active sites and 6FP, respectively, and [ES] is the concentration of the XOD−$6FP_1$ complex at time t. As is shown in Figure 3a, the formation of the XOD−$6FP_1$ complex is nearly completed within 200 ms after mixing XOD and 6FP. Rearranging the data in a plot of $([S]_0 - [ES])/([E]_0 - [ES])$ vs time t and then fitting these data according to eq 6, one obtains a value of 1.09×10^6 M^{-1} s^{-1} for the intrinsic rate of complex formation, k (see Figure 3b). The intrinsic rate constant k_1 is larger than a reported value of 1.6×10^5 M^{-1} s^{-1} derived from a steady-state experiment for 6FP binding to XOD (*33*) but is close to a k_1 value of 2×10^6 M^{-1} s^{-1} for xanthine binding to XOD (*34*). By definition, $K_i = (k_2 + k_3)/k_1$, and therefore, the value of K_i for the inhibition of XOD by 6FP is equal to 0.94 nM ($1.02 \times 10^{-3}/(1.09 \times 10^6)$) at 22 °C. The value of k_1 so obtained is for the binding of the first 6FP to one of the XOD active sites with the other active site unoccupied. Notice that the value of k_1 is 9 orders of magnitude larger than the value of $(k_2 + k_3)$ and k_2 is on the order of 10^{-4} s^{-1}; binding of 6FP to XOD is quantitative and irreversible. The XOD−$6FP_1$ complex will not dissociate back to free 6FP and XOD within a time scale of ca. 238 min at 22 °C. In other words, the reactants (6FP and XOD) and the products (the XOD−$6FP_1$ complexes) in eq 1 are *not in dynamic equilibrium* (nor in a steady-state condition) within ca. 238 min after mixing 6FP and XOD at 22 °C. Therefore, the traditional steady-state method of the Lineweaver−Burk plot is not an appropriate tool for obtaining the values of K_i or K_m for very strong binding but very slowly dissociating or reacting substrates.

To investigate the cooperativity between the two XOD active sites, the rate of conversion of 6FP to 6CP was measured in the presence of different equivalents of 6FP. Figure 4a displays the lag time, as well as the onset decay, of the $A_{620\ nm}$ absorbance in the presence of different amounts of 6FP. Since k_1 is 10 orders larger than k_2 and k_2 is on the order of 10^{-4} s^{-1}, binding of the first 6FP to XOD active sites to form XOD−$6FP_1$ is quantitative and irreversible. All XOD subunits will be converted to the forms of XOD−$6FP_1$

and XOD−6FP$_2$, when the amount of 6FP is greater than 1 equiv, leading to $[XOD]_{free} \cong 0$. Because the concentration of free XOD is almost zero, eq 2 becomes $d[XOD-6FP]/dt = -(k_2 + k_3)[XOD-6FP_1]$. By fitting the decay of the $A_{620\ nm}$ in Figure 4a to a single-exponential function, we obtain roughly the same $(k_2 + k_3)$ values of 1.75×10^{-3} s^{-1} for all four curves depicted in Figure 4a. Since XOD has two active sites, the decay of the $A_{620\ nm}$ (i.e., conversions of 6FP to 6CP from XOD−6FP$_1$ and XOD−6FP$_2$) should be two exponentials when the amount of 6FP is larger than 0.5 equiv. The two-exponential decays will be the same in the case of independent catalysis between the two XOD subunits and will be different when cooperative interactions exist between the two catalytic subunits. The decay of the $A_{620\ nm}$ in Figure 4a can be fitted reasonably well by a single-exponential function, indicating that the two expected exponential functions are probably on the same order, if there is any difference. The value of the fitted decay rate of 1.75×10^{-3} s^{-1} in Figure 4a can only be treated as an approximated and averaged 6FP/XOD complex disappearance rate. This averaged decay rate (or the XOD/6FP disappearance rate) is 1.7-fold larger than the XOD−6FP$_1$ disappearance rate of 1.02×10^{-3} s^{-1}, suggesting that the second exponential function (i.e., the disappearance rate for XOD−6FP$_2$) is probably a few fold larger than that for XOD−6FP$_1$. In Figure 4, another important information is the lag time prior to the decay of the $A_{620\ nm}$. The observed lag time is 0, 6.5, 11, and 16 min for 1, 2, 3, and 4 equiv of 6FP, respectively. In the following section, the lag time will be analyzed according to the independent catalysis model. It will be shown that the predicted lag time from the independent catalysis model was not observed and, therefore, the independent catalysis model does not operate in the current XOD system. The analysis is as follows. Since the XOD molecule has two catalytic subunits, there should be two sets of kinetic parameters, (k_1, k_2, k_3) and (k_1', k_2', k_3'), for binding and catalysis of XOD−6FP$_1$ and XOD−6FP$_2$, respectively. The kinetic parameters (k_1', k_2', k_3') and (k_1, k_2, k_3) are the same in the case of the independent catalysis model but are different in the case of the cooperative catalysis model. In the earlier sections, we have obtained the values of (k_1, k_2, k_3) for binding of the first 6FP to XOD. Since the value of k_1 is ca. 9 orders of magnitude larger than $(k_2 + k_3)$ and k_2 is approximately 1 order of magnitude smaller than k_3, binding of the first 6FP to XOD active sites to form XOD−6FP$_1$ is quantitative and irreversible and the major exit channel of the bound 6FP is conversion to 6CP. Under the condition of independent catalysis, binding of the second 6FP to the active site of XOD−6FP$_1$ is the same as the first 6FP, that is, quantitative and irreversible. In this case, the disappearance rates of 6FP to 6CP for XOD−6FP$_1$ and XOD−6FP$_2$ are the same and are 1.02×10^{-3} s^{-1}, and the enzyme is always operating at a V_{max} condition when the amount of 6FP is larger than 1 equiv. The above predicted disappearance rate of 1.02×10^{-3} s^{-1} for XOD/6FP complex, based on the independent catalysis model, is slower than the experimentally observed value of $\sim 1.75 \times 10^{-3}$ s^{-1} in Figure 4a, suggesting that cooperative interaction exists between the two XOD subunits. Regarding the lag time (see Figure 4a,b), the $A_{620\ nm}$ absorbance will not start to decay until all free 6FP in solution is converted to 6CP. Therefore, the lag time prior to the decay of the $A_{620\ nm}$ absorbance will be proportional to the amount of 6FP added. The more 6FP added, the longer the lag time would be. The lag time is also related to the 6FP to 6CP conversion rate (or the decay of the $A_{620\ nm}$ absorbance). A faster conversion rate will result in a shorter lag time required to convert all free 6FP in solution to 6CP before the onset decay of the $A_{620\ nm}$ absorbance (or, the onset decrease of the [ES]) occurs. Under the condition of the independent catalysis, binding of the first and the second 6FP to XOD active sites are both quantitative and irreversible. When 6FP is in large excess, all XODs are in the form of XOD−6FP$_2$, that is, $[ES] = [XOD]_{mo}$. The 6CP formation rate is now equal to the product of k_3 and $[XOD]_{mo}$, that is,

$$\Delta[P]/\Delta t = k_3[XOD]_{mo} \quad \text{or} \quad \Delta t = k_3^{-1}\{\Delta[P]/[XOD]_{mo}\} \tag{7}$$

Under the condition of excess 6FP and the condition of independent catalysis, the unit lag time (Δt) for the conversion of 1 equiv of 6FP to 6CP will be equal to $k_3^{-1} = (0.95 \times 10^{-3}\ s^{-1})^{-1} = 17.5$ min, since 1 equiv of 6CP $= \Delta[P] = [ES] = [XOD]_{mo}$, that is, $\Delta[P] = [XOD]_{mo}$ in eq 7. The independent catalysis model predicts that the unit lag time should be a constant value of 17.5 min in the presence of an additional equivalent of 6FP. That is to say, according to the independent catalysis model, the lag time in Figure 4a,b should be 0, 17.5, 35, and 52.5 min for 1, 2, 3, and 4 equiv of 6FP, respectively. Experimentally, the observed lag time of 0, 6.5, 11, and 16 min is ~3-fold shorter than the values predicted by the independent catalysis model. Therefore, the independent catalysis model is not the working model for the XOD system. The much shorter lag time and the faster decay rates observed in Figure 4 are consistent with the hypothesis that the 6FP to 6CP conversion rate of XOD−6FP$_2$ is faster than that for XOD−6FP$_1$, that is, binding of a 6FP can accelerate the 6FP to 6CP conversion rate at the adjacent XOD active site. Although we do not have the exact k_1' and k_2' values for binding of the second 6FP, the k_2' value is most probably very small, similar to k_2, and is many orders smaller than k_1' such that binding of the second 6FP to XOD−6FP$_1$ active site is also quantitative and irreversible. This argument is supported by nearly the same (within limited experimental errors) saturated $A_{620\ nm}$ absorbances of XOD solutions in the presence of 1, 2, 3, and 4 equiv of 6FP (see Figure 4a). The faster decay rate and the shorter lag time than the values predicted by the independent model are probably due to the contribution from a faster k_3' value than k_3. The value of k_3' will be deduced from Figure 5.

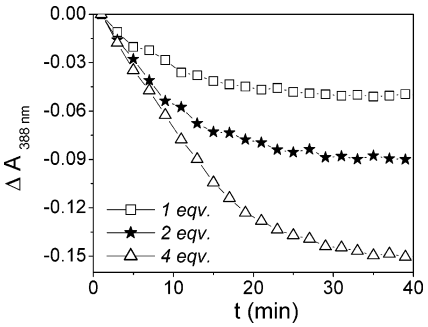

FIGURE 5: The absorbance at 388 nm as a function of time in the presence of 1, 2, and 4 equiv of 6FP in a XOD solution. The experimental conditions are the same as those in Figure 4.

As discussed above, the conversion rate of 6FP to 6CP in XOD−$6FP_2$ seems to be faster than the conversion rate in the XOD−$6FP_1$ complex. This phenomenon of cooperative interaction−accelerated 6FP to 6CP conversion is also illustrated in Figure 5, where the formation of 6CP was monitored at the 388 nm bleaching from a XOD solution containing 1, 2, and 4 equiv of 6FP, respectively. In Figure 5, the initial slope (i.e., the formation rate of 6CP) becomes larger when higher equivalents of 6FP are present in the XOD solution, indicating a faster 6FP to 6CP conversion rate at higher equivalents of 6FP. At very low equivalents of 6FP (e.g., 0.1 equiv, the condition in Figure 1), the $A_{388\ nm}$ bleaching with a rate constant of k_3 is solely due to contribution from the XOD−$6FP_1$. When the concentration of 6FP is larger than 1 equiv, the bleaching of the $A_{388\ nm}$ (i.e., the 6CP formation rate) is composed of two exponential functions with rate constants of k_3 and k_3'. At higher 6FP equivalents, the contribution of the XOD−$6FP_1$ component diminishes and the XOD−$6FP_2$ component becomes more and more dominant. By dividing the initial slope in Figure 5 by $\Delta\epsilon_{388\ nm,6CP-6FP}$ and $[XOD]_{mo}$, we obtained a 6FP to 6CP conversion rate of 2.8×10^{-3} s^{-1} from the solution containing 4 equiv of 6FP. This conversion rate of 2.8×10^{-3} s^{-1} is ∼2.95-fold larger than the k_3 value of 0.95×10^{-3} s^{-1} for 6FP to 6CP conversion from XOD−$6FP_1$. Although we do not have the value of K_i' for the second 6FP, binding of the second 6FP to the active site of XOD−$6FP_1$ is probably similar to binding of the first 6FP, that is, nearly quantitative and irreversible. This assumption is supported by the nearly the same maximum $A_{620\ nm}$ absorbances of a XOD solution in the presence of 1, 2, 3, and 4 equiv of 6FP (see Figure 4a). Therefore, nearly all XOD exists in the form of XOD−$6FP_2$ in the presence of 4 equiv of 6FP. The value of 2.8×10^{-3} s^{-1}, thus, corresponds to the 6FP to 6CP conversion rate of XOD−$6FP_2$ with, if there is any, very small contribution from XOD−$6FP_1$. Notice that the 6FP to 6CP conversion rate of 0.95×10^{-3} s^{-1} for XOD−$6FP_1$ is ∼3-fold smaller than the above 2.8×10^{-3} s^{-1}. The greater the contribution from the XOD−$6FP_1$ species, the slower the observed 6FP to 6CP conversion rate will be (see results in Figure 5). Therefore, without a doubt, the 6FP to 6CP conversion rate from XOD−$6FP_2$ is larger than that for the XOD−$6FP_1$. The above data clearly show that the preoccupation of a 6FP at a XOD active site can accelerate the 6FP to 6CP conversion rate of the adjacent active site by ∼2.95-fold. The 2.95-fold larger k_3' value than k_3 matches quite well with the 3-fold shorter observed lag time as compared to the values calculated from the independent model (i.e., based on the rate constant k_3).

To provide more evidence for cooperative interactions between XOD subunits, the effects of heterosubstrates on the conversion of the XOD−$6FP_1$ complex were studied. In the presence of 1 equiv of 6FP, all XOD active sites will be converted to be in the forms of XOD−$6FP_1$ and XOD−$6FP_2$, since k_1 is 9 orders of magnitude larger than ($k_2 + k_3$) and k_2 is on the order of 10^{-4} s^{-1}. The decay of $A_{620\ nm}$ for the as-formed (without column separation) XOD−$6FP_n$ ($n = 1$ or 2) complexes was monitored in the absence and the presence of other substrates (such as xanthine or xanthopterin). As time goes by, more and more XOD−$6FP_2$ was converted to XOD−$6FP_1$, leading to more and more XOD active sites becoming available to other free substrates in the solution. If the two XOD active sites are catalytically independent from each other, the decay rate of the $A_{620\ nm}$ absorbance would remain unchanged whether the adjacent active site of XOD−$6FP_1$ was occupied by other substrates or not. As is shown in Figure 6, the presence of xanthine significantly enhances the decay rate of the $A_{620\ nm}$ absorbance (i.e., the conversion rate of 6FP to 6CP). On the other hand, the presence of a 6,6-ring substrate, xanthopterin, leads to a slower conversion rate of 6FP to 6CP. The data in Figure 6 demonstrate unambiguously that cooperative interactions exist between the two XOD active sites. The independent catalysis model cannot explain the observations shown above in Figures 4−6. Notice that the 6FP molecules in the active sites of XOD will not be replaced by the subsequently added substrates, since k_2 for 6FP is on the order of 10^{-4} s^{-1} (i.e., the system is *not in a state of dynamic equilibrium* within the time scale of 238 min at 22 °C). Even if the system were in a dynamic equilibrium, one would expect to observe an immediate and complete drop in the intensity of the $A_{620\ nm}$ upon addition of large amount of other competing substrates, rather than the results depicted in Figure 6. Binding of xanthine to the XOD active sites does not generate a long-lived, stable [ES] complex, and thus no increase in the $A_{620\ nm}$ is observed. Mixing of 20 μM xanthopterin alone with XOD does not generate a long-lived ES complex, and thus no increase in the $A_{620\ nm}$ absorbance is observed. Addition of a high concentration (e.g., 100 μM) of xanthopterin to the XOD active sites does result in a very short time formation of ES complex and thus an increase (not a decrease) over a very short time (ca. 1 min) in the absorbance at 620 nm. The observations in Figure 6 cannot be explained by the independent catalysis model but are consistent with the cooperative interaction model. In addition to the XOD/6FP system, another well-known nondynamic equilibrium system is the very long-lived stable alloxanthine−XOD(Mo^{4+}) complex system, which has a dissociation half-life of >5 h in air at room temperature. As shown in Figure 7, the presence of xanthine significantly accelerates the dissociation rate of the alloxanthine from the XOD(Mo^{4+}) active site, and thus results in a much faster recovery rate of the XOD

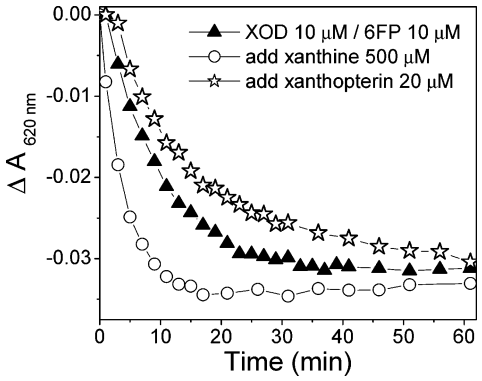

FIGURE 6: Bleaching in the intensity of the 620 nm absorbance (i.e., a measure of the amount of the XOD−$6FP_n$ ($n = 1$, 2) complexes) in the absence (▲) and the presence of 500 μM xanthine (○) and 20 μM xanthopterin (☆). 6FP (10 μM) was added to a XOD solution (10 μM, concentration of functional active sites) in 0.1 M phosphate at pH 7.5 and 22 °C. An aliquot of xanthine (final concentration, 500 μM) or xanthopterin (final concentration, 20 μM) was then added to the solution (after the formation of the XOD−6FP complexes had occurred), followed by repeated scanning (every 2 min) to monitor the decay in the 620 nm absorbance.

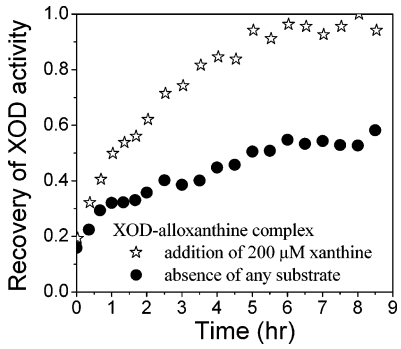

FIGURE 7: The recovery of the XOD activity from an alloxanthine−XOD(Mo^{4+}) complex solution in 0.1 M phosphate at pH 7.5 in the absence (●) and the presence (☆) of 200 μM xanthine at 22 °C in air. The alloxanthine−XOD(Mo^{4+}) complex solution was obtained by mixing a XOD solution with excess amount of allopurinol, followed by passing the solution through a Sephadex G-25 column to isolate the alloxanthine−XOD(Mo^{4+}) complex. The XOD activity was monitored by removing an aliquot of the XOD solution every 20 min to examine for its activity using xanthine as a substrate.

activity. The results in Figure 7 again demonstrate that very strong cooperative interactions exist between the two XOD active sites.

Previously, it was reported in 1949 that binding of 1 equiv of 6FP leads to deactivation of more than one unit of XOD activity (*31*). However, the structure of XOD homodimer was not known at that time, and thus the negative cooperative interactions between XOD active sites were never taken into consideration. It was proposed that XOD from commercial sources might contain three different forms, namely, doubly active dimer, mixed dimer, and doubly inactive dimer. The inactive unit could be in the desulfo form (*21*) or be lacking the molybdenum metal (*22*, *23*). The doubly active dimers could be separated from the other two forms via a Sepharose 4B−folate gel column (*24*). In the current study, the XOD sample was purified by a Sepharose 4B−folate affinity column to have ~85% activity. Although other components, such as doubly inactive and mixed dimer, may exist in the final enzyme samples and allow binding of substrates as well, these "impurities" will not produce the cooperative catalysis phenomenon due to the absence of catalysis sites. Only can the doubly active dimers produce the cooperative catalysis phenomenon. The presence of other "impurities", in fact, might make the cooperative effects less pronounced by diluting the effects of cooperative interactions produced from these doubly active dimers. Therefore, high purity of the enzyme sample is not a prerequisite factor for the observation of the cooperative catalysis in multimeric enzymes. In fact, the above cooperative interactions between the two XOD subunits can also be observed from commercial XOD samples with 45% purity.

In the literature, the cooperative binding and catalysis phenomena have been observed in many biological systems. For example, binding of an oxygen molecule to hemoglobin (*35*) can promote binding of another oxygen molecule. Another example of allosteric interactions between different binding sites is aspartate transcarbamoylase (*36*). Upon binding of a regulator (either ATP or CTP) at the regulatory site, there are significant changes in both the protein conformation near the active site and the enzyme's ability to bind a substrate. Many other examples have been discussed in the Introduction section. Similar to the phenomenon of regulator-binding-induced enzyme conformation changes, binding of a substrate at an active site of oligomeric enzymes could also result in significant conformation changes near the enzyme active sites. This type of substrate-binding-induced protein conformation changes are, however, dynamic in nature and are retained only during the time period of substrate binding at an active site. To have such dynamic cooperative interactions among different subunits show up in kinetic data, it requires simultaneous binding of two substrates at adjacent enzyme active sites. When the catalysis rate is too fast or when the K_m value of a substrate is too large, the substrate retention time at an active site is too short to allow simultaneous binding of two substrate molecules at adjacent active sites, leading to difficulty observing the cooperative interactions kinetically. This explains why so many oligomeric enzymes, including the XOD system, are thought to be "noncooperative". A very high substrate concentration condition will favor simultaneous binding of more than one substrate molecule at active sites and thus the occurrence of cooperative interactions among catalytic subunits. Previously, it was reported that the catalysis rate becomes slower at very high xanthine concentrations, a phenomenon known as "substrate inhibition" (*4*, *5*, *37*). This phenomenon was formerly rationalized by assuming binding of substrates to a presumed regulatory site at very high substrate concentrations (*4*). The XOD crystal structure, however, depicts the absence of such a regulatory site. To rationalize the "substrate inhibition" phenomenon, it was also postulated that when the amount of substrate is in excess, the enzyme in reduced form might form a stable inactive enzyme−substrate complex, analogous to the alloxanthine−XOD(Mo^{4+}) complex (*5*, *37*). Such a putative inactive enzyme−substrate complex was, however, never isolated. The "substrate inhibition" phenomenon can now be well rationalized by the cooperative interactions exerted between two adjacent XOD active sites. Besides the very high substrate concentration condition, an alternative to increase the substrate retention time at enzyme active sites is to use tight binding but slow catalyzing substrates. The long substrate retention time of such inhibitor-like substrates at enzyme active sites significantly prolongs the time period of the binding-induced protein conformational changes, allowing the occurrence of simultaneous binding of two substrates at adjacent active sites. Simultaneous binding of two substrates at adjacent active sites is prerequisite for the operation of cooperative interactions among catalytic subunits. In this paper, we have demonstrated for the first time that tight binding but slow catalyzing substrates, such as 6FP, are very useful tools for the studies of the cooperativity in "noncooperative" oligomeric enzymes.

In conclusion, our experimental evidence clearly shows that the two XOD subunits are highly interrelated to each other in both binding and catalysis. Binding of a 6FP accelerates the catalysis rate of a preoccupied 6FP at the other active site. The presence of different substrates (at low concentrations) in the solution can also change the conversion rate of 6FP to 6CP at the XOD active sites. These observations demonstrate unambiguously that the two active sites of XOD are highly dependent on one another for both binding and catalysis. It is necessary now to reexamine the literature data regarding the XOD catalysis kinetics and models, especially when dealing with these tight-binding

slow-conversion substrates, by taking into account the effects of cooperative interactions between the XOD subunits.

ACKNOWLEDGMENT

The authors express their appreciation to Professor Sunney I. Chan (Institute of Chemistry, Academia Sinica, Taiwan) for allowing the use of his stopped-flow spectrometer.

REFERENCES

1. Enroth, C., Eger, B. T., Okamoto, K., Nishino, T., and Pai, E. F. (2000) Crystal structures of bovine milk xanthine dehydrogenase and xanthine oxidase: Structure-based mechanism of conversion, *Proc. Natl. Acad. Sci. U.S.A. 97*, 10723−10728.
2. Hille, R., and Massey, V. (1986) The equilibration of reducing equivalents within milk xanthine-oxidase, *J. Biol. Chem. 261*, 1241−1247.
3. Hille, R., and Anderson, R. F. (1991) Electron-transfer in milk xanthine-oxidase as studied by pulse-rediolysis, *J. Biol. Chem. 266*, 5608−5615.
4. Hofstee, B. H. J. (1955) On the mechanism of inhibition of xanthine oxidase by the substrate xanthine, *J. Biol. Chem. 216*, 235−244.
5. Rubbo, H., Radi, R., and Prodanov, E. (1991) Substrate inhibition of xanthine oxidase and its influence on superoxide radical production, *Biochim. Biophys. Acta 1074*, 386−391.
6. Caligiuri, M. G., and Bauerle, R. (1991) Subunit communication in the anthranilate synthase complex from salmonella-typhimurium, *Science 252*, 1845−1848.
7. Tricot, C., Schmid, S., Baur, H., Villeret, V., Dideberg, O., Haas, D., and Stalon, V. (1994) Catabolic ornithine carbamoyltransferase of Pseudomonas-Aeruginosa-Changes of allosteric properties resulting from modifications at the C-terminus, *Eur. J. Biochem. 221*, 555−561.
8. Koshland, D. E., Jr. and Hamadani, K. (2002) Proteomics and models for enzyme cooperativity, *J. Biol. Chem. 277*, 46841−46844.
9. Levitzki, A., Stallcup, W. B., and Koshland, D. E., Jr. (1971) Half-of-the-Sites Reactivity and the Conformational States of Cytidine Triphosphate Synthetase, *Biochemistry 10*, 3371−3378.
10. Scrutton, N. S., Deonarain, M. P., Berry, A., and Perham, R. N. (1992) Cooperativity induced by a single mutation at the subunit interface of a dimeric enzyme: glutathione reductase, *Science 258*, 1140−1143.
11. Kuo, L. C., Zambidis, I., and Caron, C (1989) Triggering of allostery in an enzyme by a point mutation: Ornithine transcarbamoylase, *Science 245*, 522−524.
12. Shyur, L, Aleshin, A. E., Honzatko, R. B., and Fromn, H. J. (1996) Site-directed Mutagenesis of residues at subunit interfaces of Porcine Fructose-1,6-bisphosphatase, *J. Biol. Chem. 271*, 3005−3009.
13. Santamaria, B., Estevez, A. M., Martinez-Costa, O. H., and Aragon, J. J. (2002) Creation of an allosteric phosphofructokinase starting with a nonallosteric enzyme- The case of Dictyostelium disceideum phosphofructokinase, *J. Biol. Chem. 277*, 1210−1216.
14. MacRae, H., Hanna, E., Ho, J. D., Fisher, A. J., and Segel, J. H. (2002) Induction of positive cooperativity by amino acid replacement within the C-terminal domain of Penicillium Chrysogenum ATP sulfurylase, *J. Biol. Chem. 275*, 36303−36310.
15. Aghajanian, S., and Engel, P. C. (1998) Use of protein engineering to explore subunit interactions in an allosteric enzymes: construction of inter-subunit hybrids in Clostridium symbiosum glutamate dehydrogenase, *Protein Eng. 11*, 569−575.
16. Hurley, T. D., Perez-Miller, S., and Breen, H. (2001) Order and disorder in mitochondrial aldehyde dehydrogenase, *Chem.-Biol. Interact. 130*, 3−14.
17. Ricci, G., Lobello, M., Caccuri, A. M., Pastore, A., Naccetelli, M., Parker, M. W., and Federici, G., (1995) Site-directed mutagenesis of human glutathione transferase P1-1-Mutation of Cys-47 induces a positive cooperativity in glutathione transferase P1-1, *J. Biol. Chem. 270*, 1243−1248.
18. Cupp, J. R., and McAlister-Henn, L. (1993) Kinetic analysis of NAD^+-isocitrate dehydrogenase with altered isocitrate binding sites: Contribution of IDH1 and IDH2 subunits to regulation and catalysis, *Biochemistry 32*, 9323−9328.
19. Kuo, L. C., Lipscoomb, W. N., and Kantrowitz, E. B. (1982) Zn^{2+}-induced cooperativity of Escherichia coli ornithine transcarbamoylase, *Proc. Natl Acad. Sci. U.S.A. 79*, 2250−2254.
20. Foreman, J. E., and Niehaus, W. G., Jr. (1985) Zn^{2+}-induced cooperativity of mannitol-1-phosphate dehydrogenase from Aspergillus parasiticus, *J. Biol. Chem. 260*, 10019−10022.
21. Massey, V., and Edmondson, D. (1970) On the mechanism of inactivation of xanthine oxidase by cyanide, *J. Biol. Chem. 245*, 6595−6598.
22. Hart, L. I., McGartoll, M. A., Chapman, H. R., and Bray, R. C. (1970) The composition of milk xanthine oxidase, *Biochem. J. 116*, 851−864.
23. Massey, V., Brunby, P. E., Komai, H., and Palmer, G. (1969) Studies on milk xanthine oxidase, *J. Biol. Chem. 244*, 1682−1691.
24. Nishino, T., and Tsushima, K. (1986) Interaction of milk xanthine-oxidase with folic-acid- inhibition of milk xanthine-oxidase by folic-acid and separation of the enzyme into 2 fractions on Sepharose 4B/folate gel, *J. Biol. Chem. 261*, 1242−1246.
25. Massey, V., Brumby, P. E., and Komai, H. (1969) Studies of milk xanthine oxidase: some spectral and kinetic properties, *J. Biol. Chem. 244*, 1682−1691.
26. Avis, P. G., Bergal, P., and Bray, B. C. (1955) Cellular constituents. The chemistry of xanthine oxidase. Part I. The preparation of a crystalline xanthine oxidase from cow's milk, *J. Chem. Soc.*, 1100−1104.
27. Massey, V., Komai, H., Elion, G. B., and Palmer, G. (1970) On the mechanism of inactivation of xanthine oxidase by allopurinol and other pyrolo[3,4-dipyrimidine], *J. Biol. Chem. 245*, 2837−2844.
28. Morell, D. B. (1952) The nature and catalytic activities of milk xanthine oxidase, *Biochem. J. 51*, 657−666.
29. Woodle, M., Zhang, J. W., and Mauzerall, D. (1987) Kinetics of charge-transfer at the lipid bilayer water interface on the nanosecond time scale, *Biophys. J. 52*, 577−586.
30. Hille, R., and Massey, V. (1981) Tight-binding inhibitors of xanthine-oxidase, *Pharm. Ther. 14*, 249−263.
31. Lowry, O. H., Bessey, O. A., and Crawford,E. J. (1949) Pterine oxidase, *J. Biol. Chem. 180*, 399−410.
32. Watanabe, K., Arai, T., Mori, H., Nakao, S., Suzuki, T., Tajima, K., Makino, K., and Mori, K. (1997) Pterin-6-aldehyde, an inhibitor of xanthine oxidase, has superoxide anion radical scavenging activity, *Biochem. Biophys. Res. Commun. 233*, 447−450.
33. Spector, T., and Perone, R. (1984) Folic acid does not inactivate xanthine oxidase, *J. Biol. Chem. 259*, 10784−10786.
34. Olson, J. S., Ballou, D. P., Palmer, G., and Massey, V. (1974) The mechanism of action of xanthine oxidase, *J. Biol. Chem. 249*, 4363−4382.
35. (a) Ackers, G. K., Doyle, M. L., Myers, D., and Daugherty, M. A. (1992) Molecular code for cooperativity in hemoglobin, *Science 255*, 54−63. (b) Gelin, B. R., Karplus, M., and Lee, A. W. M. (1983) Hemoglobin tertiary structural-Change on ligand-binding-sites role in the cooperative mechanism, *J. Mol. Biol. 171*, 489−559.
36. (a) Newell, J. O., Markby, D. W., and Schachman, H. K. (1989) Cooperative binding of the bisubstrate analogue N-(phosphonacetyl)-L-aspartate to aspartate transcarbamoylase and the heterotropic effects of ATP and CTP, *J. Biol. Chem. 264*, 2476−2481. (b) Eisenstein, E., Markby, D. W., and Schachman, H. K. (1990) Heterotropic effectors promote a global conformational change in aspartate transcarbamoylase, *Biochemistry 29*, 3724−3731.
37. Bray, R. C. (1975) in *The Enzymes* (Boyer, E. P., Ed.), Vol. XII, part B, pp 300−419, Academic Press, New York.

BI035467B